Contents lists available at ScienceDirect

Microchemical Journal

journal homepage: www.elsevier.com/locate/microc



Highly sensitive and label-free electrochemical detection of cardiac myoglobin using an Au/Co-BDC@MD-based Immunosensor

Qiaozhi Yang ^a, Weiyun Chen ^a, Jiaxin Shi ^c, Xin Huang ^a, Luwei Zhang ^d, Yunhan Zhang ^e, Yixuan Wang ^f, Yudong Wu ^a, Xin Li ^{b,g,h,i,*}, Kebin Xu ^{a,g,h,i,**}, Qi Wang ^{j,k,l}

- ^a School of Public Health, Shenyang Medical College, Shenyang 110034, People's Republic of China
- ^b School of Stomatology, Shenyang Medical College, Shenyang 110034, People's Republic of China
- ^c School of Medical Information Engineering, Shenyang Medical College, Shenyang 110034, People's Republic of China
- d Affiliated 242 Hospital, Shenyang Medical College, Shenyang 110801, People's Republic of China
- e School of Traditional Chinese Medicine, Liaoning University of Traditional Chinese Medicine, Shenyang 110847, People's Republic of China
- f The First Clinical Medical College, Shenyang Medical College, Shenyang 110034, People's Republic of China
- ⁸ Liaoning Province Key Laboratory for Phenomics of Human Ethnic Specificity and Critical Illness (LPKL-PHESCI), Shenyang 110034, People's Republic of China
- h Shenyang Key Laboratory for Phenomics, Shenyang 110034, People's Republic of China
- Shenyang Key Laboratory of Prevention and Treatment of Systemic Important Diseases Associated with Oral Diseases, Shenyang 110034, People's Republic of China
- ^j State Key Laboratory of Synthetical Automation for Process Industries, Northeastern University, Shenyang 110819, People's Republic of China
- k College of Information Science and Engineering, Northeastern University, Shenyang 110819, People's Republic of China
- ¹ Hebei Key Laboratory of Micro-Nano Precision Optical Sensing and Measurement Technology, Qinhuangdao 066004, People's Republic of China

ARTICLE INFO

Keywords: Acute myocardial infarction Electrochemical immunosensor Biomarkers Myoglobin

ABSTRACT

Myoglobin (Myo) is the earliest biomarker for the diagnosis of acute myocardial infarction (AMI). Sensitive and reliable Myo assays are essential for timely diagnosis of AMI. In this work, a label-free electrochemical immunosensor was prepared by modifying a glassy carbon electrode (GCE) with a nanocomposite material combining a two-dimensional metal-organic framework (Co-BDC,1,4-benzenedicarboxylate is abbreviated as BDC) hybridized with molybdenum disulfide (MD) nanosheets and loaded with gold nanoparticles (Au NPs). The Au/Co-BDC@MD-modified electrode exhibits good electrochemical properties and biocompatibility, contributing to excellent sensor performance. Under optimal conditions, the linear range of the proposed electrochemical sensor possessed good specificity, reproducibility and stability. Meanwhile, the amount of Myo in serum was detected with recoveries of 96.9–98.5 % (RSD, 0.31–1.02 %). Therefore, the constructed immunosensor is important for the sensitive and accurate detection of Myo and the early diagnosis of AMI.

1. Introduction

Acute myocardial infarction (AMI) is an extremely severe cardiovascular disease with high mortality, posing a significant threat to human health. Timely identification of AMI by monitoring cardiac biomarkers in the bloodstream is essential for enhancing patient survival outcomes [1]. Clinical cardiology research has shown that cardiac myoglobin (Myo) is the earliest biomarker of AMI. Its small molecular size (17.8 kDa) enables rapid release into the bloodstream (as early as 1–3 h after symptom onset), and its rapid release kinetics and predictive accuracy render Myo a crucial early detection marker for AMI [2]. Currently, the common methods for detecting Myo include fluorescence analysis [3], electrochemical detection [4,5], electrochemiluminescence analysis [6,7], and electrochemical immunosensors [8]. However, compared to label-free electrochemical immunosensors, these methods require additional labeling steps, which make the detection process more complex and expensive. Label-free electrochemical immunosensors are a more direct and efficient detection method. They directly convert the biological signal generated during the specific recognition process of antigens and antibodies into an electrical signal, thereby

 $^{^{*}}$ Corresponding authors at: School of Stomatology, Shenyang Medical College, Shenyang 110034, People's Republic of China.

^{**} Corresponding authors at: School of Public Health, Shenyang Medical College, Shenyang 110034, People's Republic of China *E-mail addresses*: httplixin@163.com (X. Li), xukebin@symc.edu.cn (K. Xu).

enabling the quantitative detection of antigens. They also have the advantages of fast detection and simple preparation [9].

In recent years, rational design of advanced nanomaterials has played a pivotal role in enhancing the sensitivity and reliability of electrochemical immunosensors. Notable examples include gourdshaped hollow PtCoNi bunched nanochains (GH-PtCoNi BNCs), which enabled label-free detection of alpha-fetoprotein (AFP) with a detection limit as low as 0.017 pg/mL, attributed to their large surface area and superior H₂O₂ reduction activity [10]. Similarly, self-supported PtPdMnCoFe high-entropy alloy with nanochain-like internetworks (HEAINN) achieved an ultrasensitive detection limit of 0.0036 pg/mL for neuron-specific enolase (NSE) [11], while PtPdCo nanoalloys anchored on hollow porous N-doped carbon fibers (HPCNFs) demonstrated a wide dynamic range (0.0001-1000 ng/mL) for procalcitonin (PCT) detection, underscoring the versatility of hybrid nanostructures in clinical bioanalysis [12]. Parallel advances in MOF-based nanozyme systems, such as the core@shell C₃N₄ NS@UiO-66 architecture developed by Khoshfetrat et al., have further demonstrated the benefits of nanoconfinement, peroxidase-like activity, and magnetic separation for ultrasensitive detection of prostate-specific antigen (0.02 pg/mL) and methylated DNA (10 pg) in complex matrices [13,14]. These studies collectively highlight the importance of structural engineering-encompassing hollow morphologies, high-entropy systems, conductive supports, and MOF encapsulation—in achieving high catalytic activity, efficient probe immobilization, and effective background suppression. Inspired by these strategies, we report a novel Au/Co-BDC@MD nanocomposite-based electrochemical immunosensor for the ultrasensitive detection of myoglobin (Myo), aiming to combine enhanced electrocatalysis with robust antibody immobilization for early diagnosis of acute myocardial infarction.

Molybdenum disulfide (MD) has a unique S-Mo-S sandwich structure and is characterized by an indirect band gap, a unique layered structure, a large specific surface area, excellent mechanical hardness and good catalytic properties [15-17]. The excellent properties of MD make it a very promising nanomaterial for use as a carrier material for the construction of label-free immunosensors [18]. However, as a substrate material, MD does not have ideal electrical conductivity. To solve this problem, researchers usually combine MD nanomaterials with additives that have higher electrical conductivity, such as carbon-based materials, precious metals, transition metals, and certain polymers. Among these, gold nanoparticles (Au NPs) have been widely applied in electrochemical immunosensors owing to their superior electronic conductivity, notable biocompatibility, and effective antibody-binding capacity. Upon integrating gold nanoparticles with MD, the resulting composite material can experience a notable enhancement in its overall conductivity, alongside an expanded total specific surface area, which augments antibody immobilization. Consequently, this improves the sensitivity and specificity in detecting target analytes. Thus, modifying MD with gold nanoparticles is an effective strategy to address the issue of MD's limited conductivity and improve the functionality of electrochemical immunosensors utilizing this material [19–21].

In addition to the conductivity issue, the high catalytic activity of MD can lead to an increase in background current, thereby reducing the sensitivity of the constructed immunosensor [22]. Therefore, it is necessary to effectively modify MD to reduce its catalytic performance while maintaining good conductivity. Metal-organic frameworks (MOFs) are rarely used directly as catalysts due to disadvantages such as low conductivity and low reactivity of metal centers [23]. However, two-dimensional (2D) MOFs (Co-BDC, 1,4-benzenedicarboxylate abbreviated as BDC) exhibit low catalytic performance for the reduction of H_2O_2 [24], making it a suitable candidate for our label-free electrochemical immunosensor design. The selection of Co-BDC is based on its unique physicochemical properties that distinguish it from other MOFs like MIL-53, aligning with the sensor's performance requirements. Specifically, unlike MIL-53—which is reported to exhibit intrinsic co-reaction acceleration effects [25]—Co-BDC's low catalytic

activity toward H₂O₂ is critical for suppressing background current in label-free detection. This characteristic allows Co-BDC to cover partial active sites of MD nanosheets, reducing unnecessary catalytic reactions of MD and minimizing background interference, which aligns with the strategy of reducing non-specific signals emphasized in [26]. Additionally, Co-BDC's 2D structure ensures good electrical conductivity when hybridized with MD: unlike some MOFs with poor conductivity that hinder electron transfer [27], Co-BDC deposited on MD surfaces does not introduce significant additional resistance, maintaining efficient charge transfer essential for enhancing signal sensitivity. Moreover, Co-BDC provides a stable platform for Au NPs via potential coordination interactions, facilitating subsequent antibody immobilization through Au-N bonds [28,29]. In contrast, MIL-53's strong co-reaction acceleration might exacerbate background current fluctuations in label-free systems, compromising detection accuracy, further supporting Co-BDC as the optimal choice. Building on these properties, an effective modification strategy was developed by combining Co-BDC with MD nanosheets. In this composite, the catalytically inactive Co-BDC covers some active sites of MD, reducing unnecessary catalytic reactions and background current, while its 2D configuration ensures the overall system retains excellent electrical conductivity—mitigating the negative impact of MD's high catalytic activity while preserving its electrical advantages, and offering a new strategy for high-performance electrochemical immunosensors. Finally, Au NPs with good electrical conductivity and biocompatibility [30,31] were attached to the Co-BDC@MD composite via Au-S bonds [32] to form an Au/Co-BDC@MD structure. This composite retains MD's large specific surface area and sensitivity, enhances conductivity through Au NPs, and reduces unwanted catalytic activity via Co-BDC's coverage of MD active sites. The high loading of Au NPs further improves substrate performance by effectively immobilizing large amounts of Ab₁ through Au—N bonds, increasing antibody binding sites, enhancing antigen capture capability, and ultimately boosting the immunosensor's sensitivity and specificity. This makes Au/ Co-BDC@MD an efficient substrate for constructing label-free electrochemical immunosensors in this study, with reference to modification methods of other electrochemical sensors [33-38].

To summarize, the synthesized Au/Co-BDC@MD nanocomposite was examined in this research through comprehensive electrochemical analysis employing techniques such as electrochemical impedance spectroscopy (EIS), cyclic voltammetry (CV), and differential pulse voltammetry (DPV). Additionally, its structural features and elemental composition were assessed using energy dispersive spectroscopy (EDS) and scanning electron microscopy (SEM). Based on Au/Co-BDC@MD as a signal amplification platform, we constructed a label-free electrochemical immunosensor.

2. Experimental section

2.1. Chemicals and materials

Tetrachloroauric acid (HAuCl₄·4H₂O) was obtained from Sinopharm Chemical Reagent Co., Ltd. L-Cysteine (C3H7NO2S), terephthalic acid (BDC), and sodium molybdate dihydrate (Na2MoO4·2H2O) were acquired from Shanghai Maclin Biochemical Technology Co., Ltd. N,Ndimethylformamide (DMF) was sourced from Tianjin Hengxing Chemical Reagent Co., Ltd. Myocardial myoglobin (Myo) and its corresponding antibody (Ab₁), cytochrome C (Cyt c), human serum albumin (HSA), and hemoglobin (Hb) were obtained from Shanghai Jizhi Biochemical Technology Co., Ltd. Bovine serum albumin (BSA) was acquired from Shanghai Aladdin Biochemical Technology Co., Ltd. Special grade foetal bovine serum (FBS) was purchased from Zhengzhou Pingrui Biotechnology Co., Ltd. The structural features of the samples were analyzed using SEM (scanning electron microscopy) and EDS (energy dispersive spectroscopy). The experiments were conducted utilizing a CHI660E electrochemical workstation (Shanghai Chenhua Instrument Co., Ltd.), with a three-electrode setup employed throughout. This configuration featured Ag/AgCl as the reference electrode, GCE as the working electrode, and a Pt wire as the counter electrode. CV measurements were carried out on several modified electrodes in a 5 mM $K_3[\text{Fe}(\text{CN})_6]$ solution, which also contained 0.1 M KNO3, at a scan rate of 0.1 V/s. The EIS measurement was carried out in a medium composed of 2.5 mM [Fe (CN)₆] $^{3-/4}$ and 0.1 M KCl, spanning a frequency spectrum from 0.01 to 10^6 Hz at an open-circuit potential of +0.385 V. DPV was executed in phosphate-buffered saline (PBS) at pH 7.4 with H_2O_2 , employing a potential sweep from -0.5 V to +1.0 V.

2.2. Preparation of au NPs

The preparation of Au NPs followed the method outlined in the literature [39]. Initially,0.2 mL of HAuCl $_4.4H_2O$ (1.0 wt%) was dispensed into a beaker, followed by the addition of 19.8 mL of secondary deionized water, which was then mixed comprehensively. A magnetic stirrer bar was inserted into the beaker, and the setup was positioned on a constant-temperature magnetic heater to ensure consistent heating and stirring until the mixture reached boiling point. During boiling, 0.3 mL (10 mg/mL) of sodium citrate was added, and stirring was maintained for 20 min, noting the solution's transformation from a pale yellow to grey and subsequently to burgundy. Ultimately, cease stirring and heating, allow the solution to cool to ambient temperature, and the resulting solution constitutes the Au NPs solution, which should be preserved in a sealed reagent bottle at 4 °C for future utilization.

2.3. Preparation of MD nanosheets

MD nanosheets were fabricated following the established protocol outlined in the literature [40,41]. A volume of 25 mL of secondary deionized water was measured, and 0.125 g of Na₂MoO₄·2H₂O crystals was carefully weighed, combined, and dissolved within a 50 mL beaker. Subsequently, the solution's pH was assessed using a pH meter, and 0.1 M hydrochloric acid was introduced to achieve a pH of 6.5. Following this,0.25 g of L-cysteine was incorporated into the beaker and fully dissolved via ultrasonication. The blend was positioned within the liner of a 50 mL reaction container, after which the steel casing was secured and fastened. The reaction assembly was subsequently transferred to an oven set at 100 °C for 1 h, followed by an increase in temperature to 200 °C, where it remained for 15 h. Upon completion of the heating process, the oven was switched off, allowing it to gradually cool to ambient temperature alongside the reaction vessel. The resulting material was rinsed three times with water using a centrifuge, dried, and subsequently utilized.

2.4. Preparation of co-BDC@MD

Reference method for the preparation of co-BDC@MD hybrid nanosheets [24]:32 mL *N*,*N*-dimethylformamide,2 mL ethanol and 2 mL deionized water were added to a screw-cap bottle. A quantity of 40.8 mg of MD nanosheets was measured and introduced into the mixture, which was then subjected to sonication for a duration of 10 min to ensure thorough blending. After mixing,0.1 mmol terephthalic acid and 0.1 mmol cobalt chloride heptahydrate were added to the screw-cap bottle and stirred until dissolved. A volume of 0.2 mL of triethanolamine was introduced into the screw-cap vial and homogenized through ultrasonication for a duration of 3 h. subsequently, the resulting mixture was rinsed three times with ethanol and deionized water, and the resultant dispersion was preserved for subsequent utilization

2.5. Preparation of au/co-BDC@MD

2.0 mL of the Co-BDC@MD mixture and 2.0 mL of the gold nanoparticle solution were added to the same centrifuge tube, mixed by ultrasound for 15 min, and then spin in a rotary mixer for 6 h. Finally,

centrifuge three times, and the resulting product is dispersed in water and stored for later use.

2.6. Electrochemical measurement

Electrochemical analyses were performed utilizing a three-electrode configuration, comprising an Ag/AgCl reference electrode, a glassy carbon working electrode (GCE, $\Phi=3$ mm), and a platinum wire counter electrode (Pt, $\Phi=0.5^*37$ mm). CV was conducted in a solution containing 20 mL of $K_3[Fe(CN)_6]$ (5.0 mM) and KNO_3 (0.1 M), at a scan rate of 0.1 V/s. The open-circuit potential was determined to be 0.385 V. The EIS was assessed in a 20 mL solution composed of KCl (0.1 M) and $[Fe(CN)_6]^{3^{-/4}}$ (2.5 mM). DPV was measured by adding 20 mL of phosphate buffer (pH = 7.4) to the electrolytic cell at an initial potential of 0.1 V and injecting H_2O_2 .

2.7. Construction of immunosensors

Initially, the surface of the GCE was refined using alumina and then thoroughly cleaned via ultrasonic treatment with secondary deionized water. Then 6 μL Au/Co-BDC@MD (3.5 mg/mL) was modified on the polished GCE and dried. In the second step, 6 μL of Ab1 (10 μg mL $^{-1}$) was incubated on the Au/Co-BDC@MD/GCE, and then the unbound Ab1 on the GCE surface was washed with PBS (pH = 7.4) and dried. In the third step, 3 μL bovine serum albumin (BSA, 1 wt%) was added dropwise to Ab1/Au/Co-BDC@MD/GCE and allowed to dry to eliminate non-specific interference. Subsequently, the BSA that was not adhered to the glassy carbon electrode was washed with PBS and subsequently dried. In the fourth step, 6 μL Myo (10 fg/mL \sim 10 ng/mL) was incubated on the BSA/Ab1/Au/Co-BDC@MD/GCE. Then, the unbound Myo was rinsed with PBS and then dried. Ultimately, the constructed immunosensor was preserved in an airtight container at a temperature of 4 °C.

3. Results and discussion

3.1. Characterisation of au/co-BDC@MD

The prepared Au/Co-BDC@MD nanomaterials were studied using SEM. Fig. 1A shows that the prepared Au/Co-BDC@MD forms a porous network structure as a whole, with pores distributed evenly. To further explore the elemental composition of Au/Co-BDC@MD, a surface scan of Au/Co-BDC@MD was performed (Fig. 1B), which showed that the material contained elements such as Co, Mo, S, and Au (Fig. 1C-F), indicating that the Au/Co-BDC@MD material was successfully modified.

3.2. Characterisation of Myo/ BSA/Ab₁/au/co-BDC@MD

Fig. 2A shows scanning electron microscopy (SEM) images of Au/Co-BDC@MD after sequential incubation with Ab₁, BSA, and Myo, Fig. 2B shows Au/Co-BDC@MD/Ab₁/BSA/Myo Surface scan image. The surface was found to have more pores and some local aggregation, with a cluster structure forming in some areas. These alterations could involve the macromolecules attaching to the material's surface via a physical adsorption process and either undergoing chemical reactions or establishing coordination bonds with the active sites on the material's surface, thus ensuring a more stable anchorage. As the protein molecules gradually deposit on the surface of the material, they not only occupy space, but also cause holes or porosity on the surface due to their unique three-dimensional structure. To confirm the successful adsorption of antigens and antibodies onto the material's surface, we examined the EDS spectra of the material prior to and following protein incubation (Fig. 2C represents the state before incubation, while Fig. 2D shows the state after incubation) and presented these as pie charts (Fig. 2E for the pre-incubation condition and Fig. 2F for the post-incubation condition). As shown in the pie charts, the oxygen content increased significantly from 4.2 % in Fig. 2E to 29.9 % in Fig. 2F. The substantial rise in oxygen

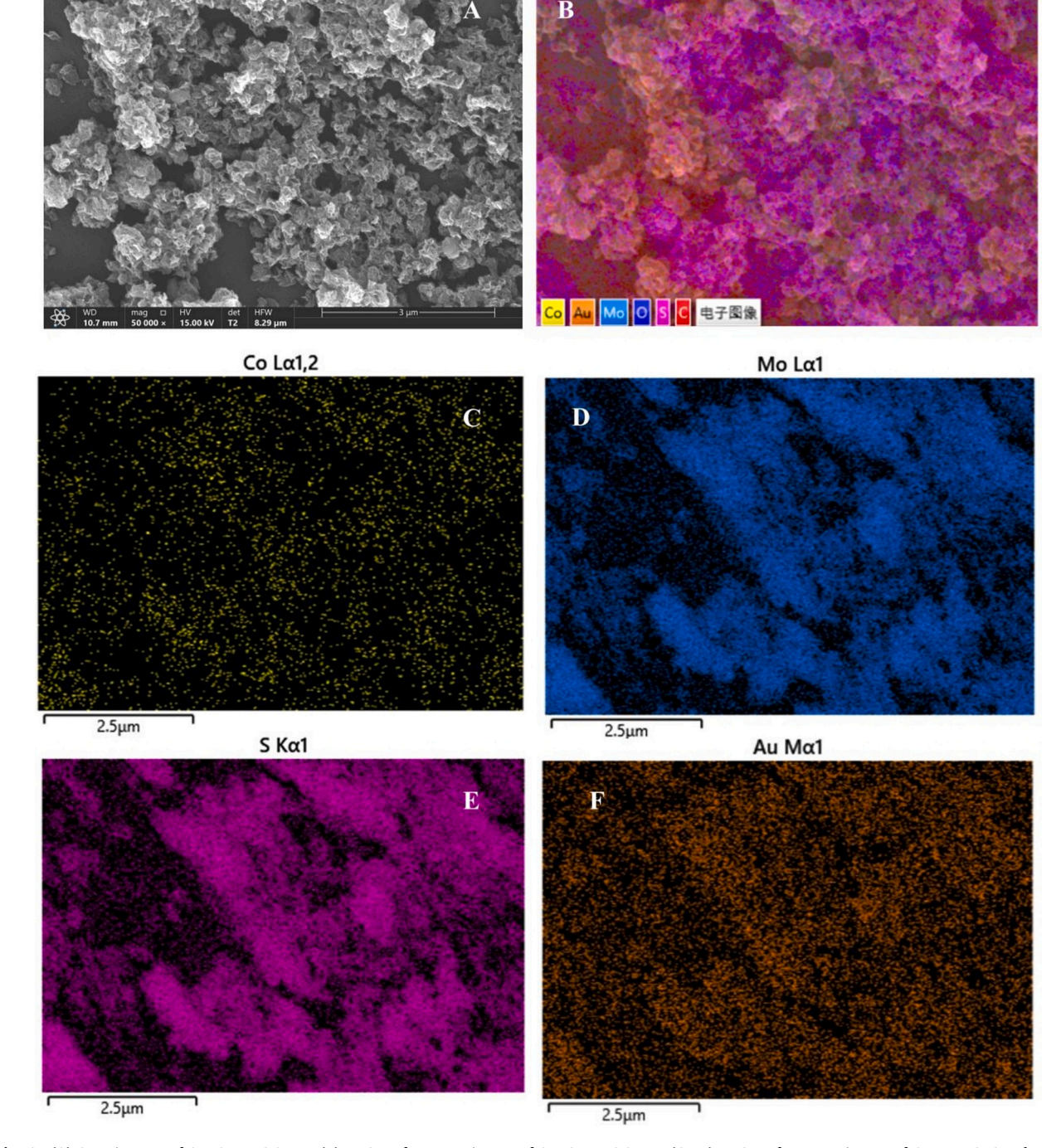


Fig. 1. (A) SEM images of Au/Co-BDC@MD. (B) EDS surface scan image of Au/Co-BDC@MD. (C—F) EDS surface scan image of Co, Mo, S, Au elements.

levels can be explained by the protein composition of both antibodies and antigens, as these molecules incorporate numerous carboxyl groups (-COOH), hydroxyl groups (-OH), and additional functional groups that contain oxygen. The abundance of such groups contributes to a higher oxygen concentration (Fig. S1). The above results show that protein molecules have indeed been successfully adsorbed onto the surface of the Au/Co-BDC@MD material. This adsorption alters both the surface morphology and chemical makeup of the material, while also demonstrating the effective attachment of antigens and antibodies.

3.3. Electrochemical characterisation

The conductivity of the substrate material affects the sensitivity of

the electrochemical immunosensor [42]. To investigate the electrical conductivity of Au/Co-BDC@MD, electrochemical impedance spectroscopy (EIS) was employed to characterize the interfacial charge transfer behavior of the modified electrode, with the conductivity evaluated by extracting the charge transfer resistance (R_{ct}). As a powerful tool for quantifying charge transfer kinetics at the electrode-electrolyte interface [43], EIS can reflect the interfacial electron transfer behavior during electrode modification through Nyquist plots, which consist of a high-frequency semicircle (related to R_{ct}) and a low-frequency linear segment (related to diffusion processes). All EIS data were fitted using Zview software with an equivalent circuit model (Rs || CPE || R_{ct}) (Fig. S3, Table S1) [44]. As shown in Fig. 3A, the Co-BDC (curve a) with a larger semicircle diameter has lower conductivity,

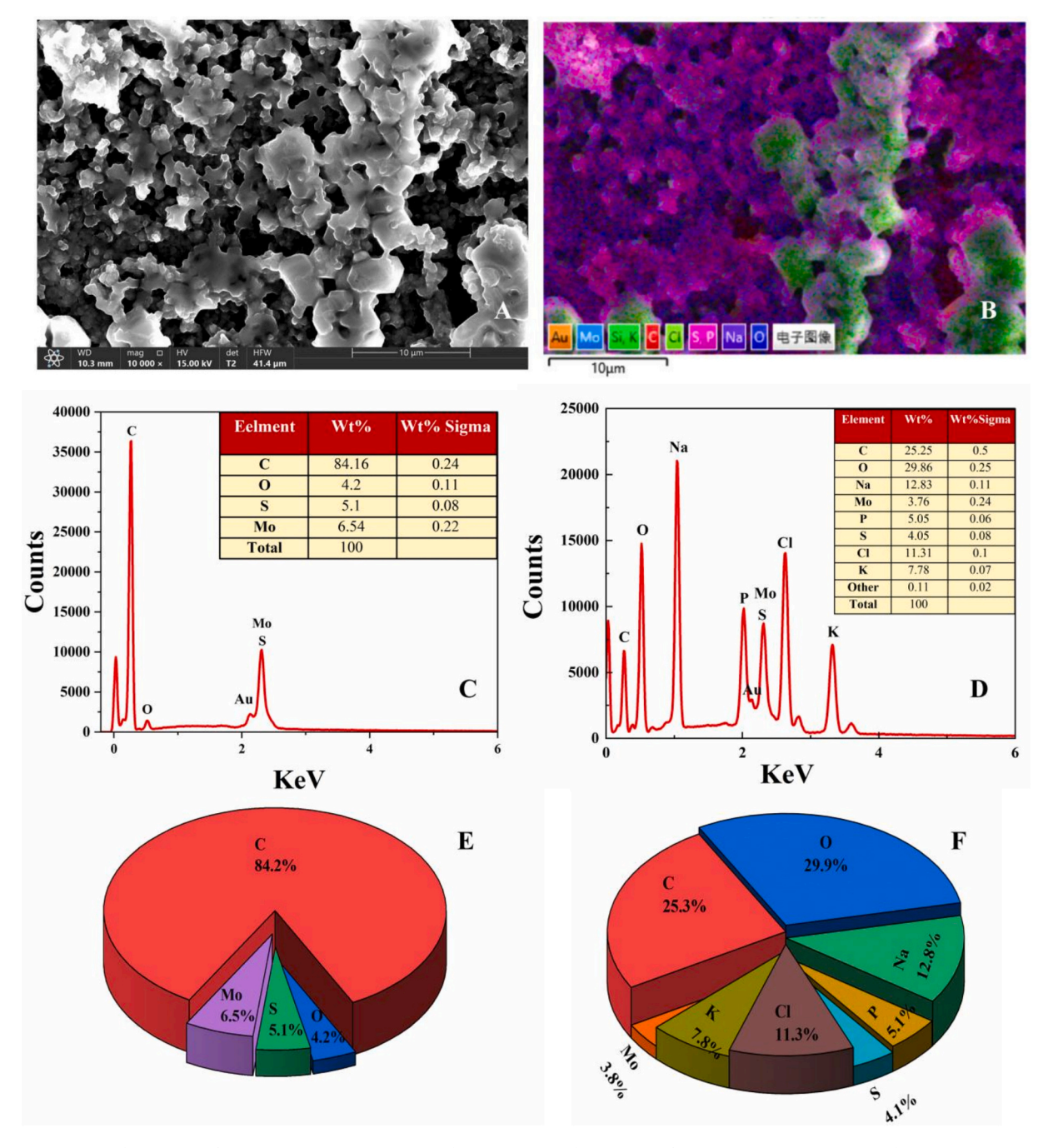


Fig. 2. (A) SEM image of Myo/BSA/Ab $_1$ /Au/Co-BDC@MD. (B) EDS surface scan image of Myo/BSA/Ab $_1$ /Au/Co-BDC@MD. (C) EDS of Au/Co-BDC@MD. (D) EDS of Myo/BSA/Ab $_1$ /Au/Co-BDC@MD. (E) Au/Co-BDC@MD element content chart. (F) Myo/BSA/Ab $_1$ /Au/Co-BDC@MD element content chart.

while the MD (curve b) with a smaller semicircle diameter has higher conductivity. The semicircle diameter of Co-BDC@MD (curve c) is smaller than that of Co-BDC (curve a) and MD (curve b), indicating that Co-BDC@MD has better conductivity. This enhancement can be attributed to the deposition of Co-BDC on the MD nanosheets, which facilitates the partial transformation of the originally 2H-phase MD nanosheets into the 1 T phase. Given that the 1 T phase of MD has higher conductivity than the 2H phase [45], the composite material formed by Co-BDC and MD nanosheets exhibits greater conductivity [40]. When Au NPs and Co-BDC@MD are further combined, a significant decrease in the composite material's resistance can be observed (curve d), indicating that Au/Co-BDC@MD possesses good electrical conductivity. Collectively, these conclusions demonstrate that Au/Co-BDC@MD, with its excellent electrical conductivity, can serve as a favorable platform for

electrochemical immunosensors.

In addition to this, the superior performance of the Au/Co-BDC@MD composite also stems from the synergistic effects between AuNPs, Co-BDC, and MD, which collectively enhance conductivity, reduce background interference, and improve biocompatibility [26]. Firstly, Co-BDC and MD exhibit synergistic regulation of catalytic activity and conductivity: Co-BDC (with low $\rm H_2O_2$ catalytic activity) covers partial active sites of MD (which inherently has high catalytic activity) [24], reducing unnecessary redox reactions and minimizing background current. Meanwhile, Co-BDC's 2D structure promotes partial transformation of MD from 2H-phase to more conductive 1 T-phase [45], and its deposition on MD does not introduce significant resistance (Table S1: Co-BDC@MD has lower Rct than Co-BDC alone), maintaining efficient electron transfer—this matches the 'activity-regulation-conductivity

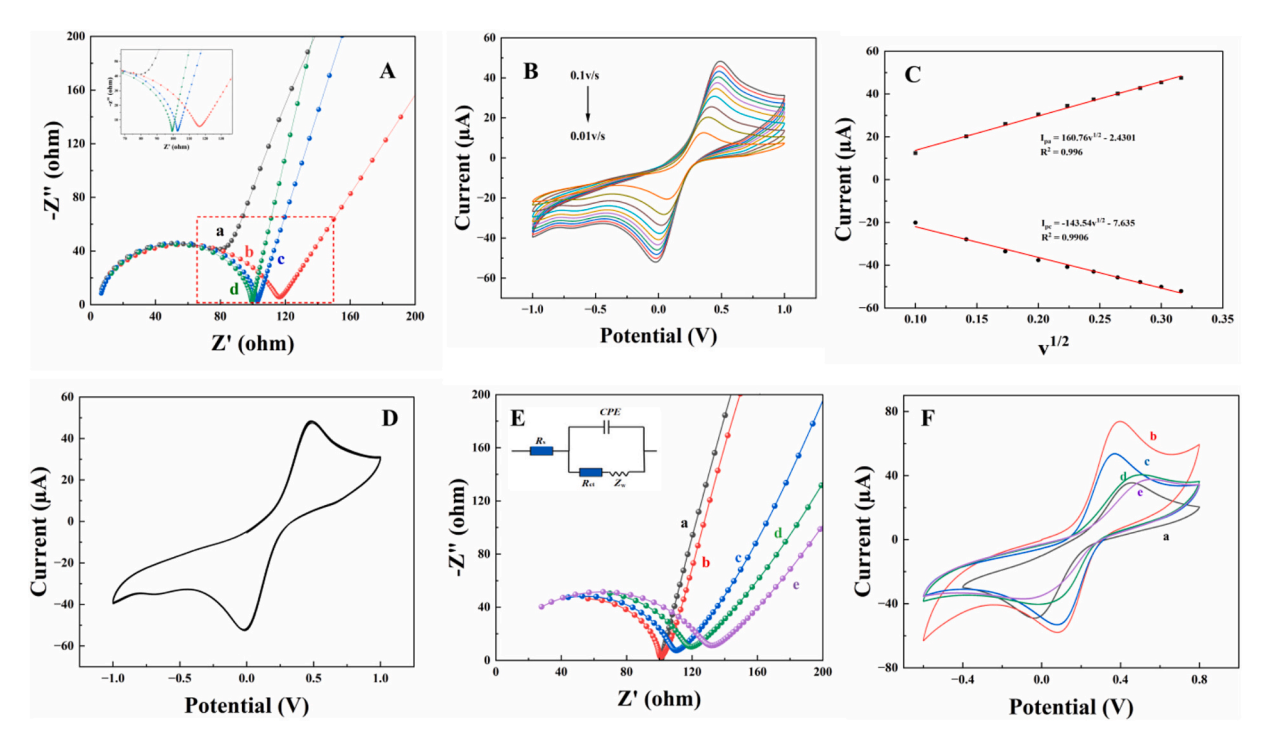


Fig. 3. EIS (A) Co-BDC (a), MD (b), Co-BDC@MD (c), Au/Co-BDC@MD (d). (B) CV diagram of Au/Co-BDC@MD modified GCE at different scan rates. (C) Inset: the relationship between ip and $v^{1/2}$ of Au/Co-BDC@MD. (D) The CV studies of Au/CO-BDC@MD under the same sweep speed (0.10 V/s) continuous sweep 30 times. (E) EIS and CV (F) of GCE (a), Au/Co-BDC@MD/GCE (b), Ab₁/Au/Co-BDC@MD/GCE (c), BSA/Ab₁/Au/Co-BDC/MD/GCE (d), Myo/BSA/Ab₁/Au/Co-BDC/MD/GCE (e).

retention' synergism described in [46]. Secondly, AuNPs synergize with Co-BDC@MD to further enhance performance: AuNPs (with excellent conductivity) form Au—S bonds with MD [32], reducing the composite's Rct from 97.17 Ω (Co-BDC@MD) to 93.62 Ω (Au/Co-BDC@MD, Table S1), consistent with the synergistic conductivity enhancement between noble metals and MOFs [47]. Additionally, AuNPs provide abundant active sites for Ab₁ immobilization via Au—N bonds [29,48], while Co-BDC's stable platform ensures uniform dispersion of AuNPs, avoiding aggregation.This 'dispersion-immobilization' synergy is essential for enhancing antigen capture efficiency [49]. Collectively, these effects enable the Au/Co-BDC@MD composite to combine low background, high conductivity, and efficient biorecognition, forming the basis for the immunosensor's high sensitivity and specificity.

CV was used to explore the electrochemical properties of Au/Co-BDC@MD. CV measurements were performed on an Au/Co-BDC@MD-modified glassy carbon electrode at scan rates of 0.01 to 0.10 V/s (Fig. 3B). As the scan rate varies, the magnitudes of the anodic and cathodic peak currents exhibit an identical variation pattern (Fig. 3C). A linear correlation is observed between the peak current (ip) and the square root of the scan rate ($\nu^{1/2}$), clearly demonstrating that the catalytic process occurring on the glass carbon electrode surface is governed by diffusion.

To investigate how material stability influences sensor performance, CV was employed to assess the stability of the Au/Co-BDC@MD composite material. The glassy carbon electrode modified with Au/Co-BDC@MD (Fig. 3D) was scanned 30 times in succession at a scan rate of 0.1 V/s. It can be seen from the image that the peak current and peak potential change insignificantly, and the current only increases by less than 2.0 % from the first cycle to the 30th cycle. This finding indicates that Au/Co-BDC@MD exhibits excellent stability, thereby establishing a foundation for the reliable detection capabilities of the sensor.

The above data show that Au/Co-BDC@MD has excellent conductivity and stability and a large specific surface area. Therefore, Au/Co-BDC@MD was selected as the signal amplification platform to construct a label-free electrochemical immunoassay sensor. The EIS analysis (Fig. 3E) served to evaluate the assembly of the immunoassay

sensor, while the Zview software facilitated the simulation of the equivalent circuit diagram to determine the respective resistance values (Table S2). Upon modifying the glassy carbon electrode with Au/Co-BDC@MD (curve b), the resulting resistance was reduced compared to the unmodified electrode (curve a), owing to the superior conductivity of Au/Co-BDC@MD and its ability to enhance electron transfer. When Ab₁ (curve c), BSA (curve d) and Myo (curve e) were sequentially deposited on the Au/Co-BDC@MD/GCE, the corresponding resistance values increased in turn. This is due to the fact that proteins, as biological macromolecules, possess significant resistance, thereby influencing the electron transfer kinetics at the glass carbon electrode interface. This aligns with the observation that the conductive carrier is separated by the protein's hydrophobic layer. Therefore, the above resistance trend proves that the preparation of the immunosensor was successful.

The amount of Ab_1 immobilized on the electrode surface was quantified using the impedance change before and after antibody immobilization, following established methods [25,27,50]. Based on the difference in charge transfer resistance (ΔRct) between the Ab_1 -modified electrode and the pre-immobilization electrode (Table S2), the surface coverage of Ab_1 (Γ) was calculated using the formula:

$$\Gamma = \frac{\Delta R_{ct} \times A}{F^2 \times C \times R}$$

where A is the electrode area, F is Faraday's constant, C is the concentration of the redox probe ([Fe(CN)₆]^{3-/4}, and R is the gas constant. The result showed $\Gamma=1.25\times10^{-10}~\text{mol/cm}^2$, indicating efficient antibody immobilization on the electrode surface.

Meanwhile, the construction of the immunosensor was verified using CV (Fig. 3F). Upon modifying Au/Co-BDC@MD on the glassy carbon electrode (curve b), the redox peak current exceeded that of the unmodified glassy carbon electrode (curve a). Then, when Ab₁, BSA, and Myo (curves c-e) were sequentially modified on the Au/Co-BDC@MD/GCE, the corresponding redox peak current change trends were consistent with the EIS plots.

3.4. Optimization of modification conditions

Within the developed electrochemical immunosensor, the current signal is influenced by the pH of the PBS, the concentration of Au/Co-BDC@MD, and the incubation duration of Myo. To optimize these parameters for optimal performance, we performed a series of systematic experiments using DPV, with each experimental condition tested in at least three independent replicates (n=3). The error bars in the corresponding figures (Fig. S2A—C) represent the standard deviation (SD) derived from these repeated measurements, ensuring the reliability and reproducibility of the optimization results.

Within a medium exhibiting high acidity or alkalinity, the functional capacity of proteins involved in antigen-antibody interactions may become compromised, thereby disrupting their association and influencing the material's catalytic efficiency and stability. Consequently, we assessed the current response across eight samples of PBS with pH levels spanning from 6.0 to 8.0 (Fig. S2A). The findings indicate that as the pH increases, the current signal initially increases before declining. The peak of the current signal is observed at a pH value of 7.4. Therefore, it can be determined that the optimal pH value of the PBS used in the experiment is 7.4. This indicates that the interaction between antigens and antibodies is most efficient under conditions near physiological pH, thus guaranteeing the material's optimal catalytic function and stability.

In the process of constructing an immunosensor, when the concentration of the substrate material exceeds a certain value, the transmission of electrons will be hindered, resulting in a weakened current signal and reduced sensitivity. The surface of the glass carbon electrode was modified with seven different concentrations of Au/Co-BDC@MD solution (0.5 mg/mL to 4.0 mg/mL) to construct a label-free electrochemical immunosensor (Fig. S2B). $\rm H_2O_2$ solution was injected slowly into 20 mL PBS (pH = 7.4) for DPV testing. Sensors fabricated with varying Au/Co-BDC@MD concentrations exhibited distinct current responses, peaking at a concentration of 3.5 mg/mL. Therefore, 3.5 mg/mL is the optimal concentration of Au/Co-BDC@MD.

To investigate whether the incubation period of Myo influences the effective binding of antigen-antibody, we examined the incubation duration of Myo under the conditions of PBS at 7.4 and a concentration of 3.5 mg/mL for Au/Co-BDC@MD (Fig. S2C). It was found that the optimal incubation time for myoglobin was 50 min. Within this time-frame, the current response attained its peak value, and a stable complex was established. During the early phase, spanning from 20 to 40 min, the current response exhibited a substantial rise as the incubation time lengthened, suggesting that myoglobin progressively adhered and interacted with the sensor's surface, leading to the formation of an increasing number of antigen-antibody complexes. When 50 min was

reached, the current response reached a peak, which means that the most stable complexes were formed at this time, and the detection sensitivity and specificity of the sensor were also optimal.

3.5. Analysis and detection

On this basis, sensors with different amounts of Myo modification were tested using DPV. Under ideal modification conditions, the associated current response signal rose as the Mvo content increased. As depicted in Fig. 4A, a linear relationship was established between lg c (where c represents the concentration of Myo) and the current signal i_p, resulting in a standard curve illustrated in Fig. 4B: I (μ A) = 2.8306 lg c + 28.7, with $R^2 = 0.987$ (n = 3). Here, c is expressed in ng/mL, and the limit of detection (LOD) was determined to be 10.03 fg/mL, calculated according to the methodology proposed by the International Union of Pure and Applied Chemistry (IUPAC) (LOD = Y blank $+3 \times SD$ blank).In contrast to the current detection approach (Table 1), the developed electrochemical immunosensor exhibits superior performance, characterized by an extended detection range and a reduced detection limit. This arises from the fact that the integration of Co-BDC and MD not only enhances charge transfer efficiency and minimizes background interference due to non-specific binding but also strengthens antibody immobilization by supplying numerous attachment points, thus enhancing the sensitivity and specificity in Myo detection.

3.6. Reproducibility, specificity and stability

Reproducibility, specificity and stability are the key factors in developing an electrochemical sensor. The superior functionality of the

Table 1Comparison of the prepared electrochemical immunosensor with other electrochemical immunosensors for detecting Myo.

Signal amplification platform	Linear range	Detection limit	References
DDAB/Au/SPE	10 ng/mL - 1780 ng/ mL	10 ng/mL	[51]
CNTs@CS-FET	1 ng/mL - 4000 ng/ mL	4.2 ng/mL	[52]
AuNPs/APTES/ITO	$10 \text{ng/mL} - 1 \mu \text{g mL}^{-1}$	2.7 ng/mL	[53]
AuNPs@rGO	$1~\text{ng/mL-}~1400~\mu\text{g}$ mL^{-1}	0.67 ng/mL	[54]
SPEs-MWCNTs	0.1 ng/mL -90 ng/mL	0.08 ng/mL	[55]
GQDs	0.01 ng/mL - 100 ng/ mL	0.01 ng/mL	[56]
Au/Co-BDC@MD	10 fg/mL - 10 ng/mL	10.03 fg/mL	This work

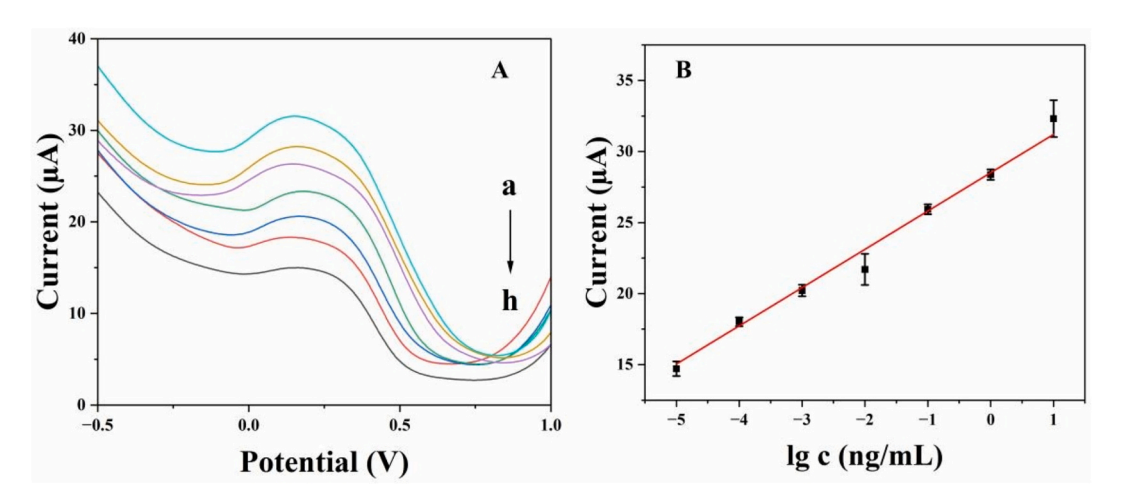


Fig. 4. (A) Currentsignal with different content of Myo:10 fg/mL,100 fg/mL,100 pg/mL,100 pg/mL,100 pg/mL,100 ng/mL,10 ng/mL,10 ng/mL. (B) The calibration curve of different content of Myo; (Error bars = SD, n = 3).

sensor has a direct impact on the precise identification of the marker. Therefore, the specificity, repeatability and stability of the electrochemical immunoassay sensor based on Au/Co-BDC@MD modification were studied by differential pulse voltammetry.

The sensor was electrochemically analyzed for reproducibility. The reproducibility of the sensor was evaluated by making electrochemical measurements with the same electrode modified five times in parallel and determining Myo solution at a concentration of 10~ng/mL. Based on the results shown in Fig. 5A, we can observe that the fluctuation of the feedback electrochemical signals during multiple measurements is extremely weak with a RSD of 1.31~%, which proves that the reproducibility of the constructed immunosensor is reliable.

To assess specificity, cytochrome C (Cyt c), human serum albumin (HSA) and hemoglobin (Hb) were assayed in the presence of Myo at the same concentration as the interfering substance (10 ng/mL). The results showed that the RSD in the presence of the interferents was 0.23 % (n=3). This indicates that the sensor can accurately and consistently identify and quantify the target analyte, Myo, both in the presence of a single interfering substance and in the presence of multiple interfering substances (Fig. 5B).

For stability tests, we stored the electrode in a PBS solution at 4 $^{\circ}$ C protected from light and performed the assay every two days. 93.24 $^{\circ}$ of its initial response was retained after 8 days of storage (n = 3,Fig. 5C). This result indicates that the constructed immunosensor proved to be stable.

Furthermore, the precision of the developed immunosensor was rigorously assessed to ensure its reliability [47,57-59]. The RSD% of the DPV responses was determined at three representative concentrations (10 fg/mL, 100 pg/mL, and 10 ng/mL) under both intra-day and interday conditions. For intra-day precision, five replicate measurements were performed on the same day. For inter-day precision, measurements were carried out on three separate days (one measurement per day). As summarized in Table S3, the intra-day RSD% values were 0.21 % (10 fg/ mL), 0.12 % (100 pg/mL), and 0.27 % (10 ng/mL), while the inter-day RSD% values were 0.56 % (10 fg/mL), 0.20 % (100 pg/mL), and 0.20 % (10 ng/mL). All RSD% values were well below the commonly accepted threshold of 5 %, indicating excellent repeatability and reproducibility across the entire analytical range. To further evaluate method robustness, a two-sample t-test (Welch's t-test, unequal variances) was performed to compare intra-day and inter-day responses at each concentration level ($\alpha = 0.05$). The results, also presented in Table S3, show p-values of 0.15 (10 fg/mL), 0.27 (100 pg/mL), and 0.54 (10 ng/ mL) — all greater than 0.05 — indicating no statistically significant differences between the intra-day and inter-day measurements. The consistently low RSD% values and non-significant t-test results collectively underscore the high consistency, reliability, and day-to-day

stability of the developed immunosensor, supporting its potential for practical clinical applications.

Low RSD values reflect the excellent reproducibility and stability of the sensor. As highlighted previously, "the microscopic homogeneity of nanomaterials is a central factor in the reduction of RSD" [60]. The homogeneous porous network structure of Au/Co-BDC@MD ensured consistent electrode modification, and optimized experimental conditions (pH = 7.4, Au/Co-BDC@MD concentration = 3.5 mg/mL, incubation time = 50 min) minimized stochastic biomolecular interactions. Additionally, efficient antibody immobilization via Au—N bonds and high specificity toward Myo reduced interference-induced signal fluctuations—consistent with the reported reduction in information noise due to biomolecular specificity on noble metal nanoparticles [61]. These performance metrics meet clinical requirements, demonstrating the sensor's potential for early diagnosis of acute myocardial infarction.

3.7. Detection of Myo in serum

The sensor was constructed and detected in fetal bovine serum (FBS) samples using DPV. The feasibility of the sensor detection in fetal bovine serum was assessed by spiked recovery experiments and data were collected (Table 2). The results showed that the RSD were $0.31-1.02\,\%$ (n = 3) and the recoveries were 96.9–98.5 %, indicating that the constructed sensors have good reliability for the detection of Myo in clinically relevant matrices.

The high recoveries close to 100 % suggest that matrix effects in serum are effectively suppressed, which is attributed to the high biocompatibility of the Au/Co-BDC@MD composite. The two-dimensional structure of Co-BDC and the hydrophilicity of Au NPs reduce non-specific adsorption, thereby avoiding competitive binding between matrix components and antibodies/antigens—consistent with the finding that "low non-specific adsorption is key to high recoveries in complex matrices" [62,63].

4. Conclusions

In this study, a sensitive and selective label-free electrochemical

Table 2Detection of Myo in fetal bovine serum samples.

Added (ng/mL)	Detection quantity (ng/mL)	RSD (%)	Rate of recovery(%)
1	0.98, 0.986, 0.984	0.31	98.3
5	4.98, 4.92, 4.88	1.02	98.5
10	9.73 , 9.77 , 9.63	0.74	96.9

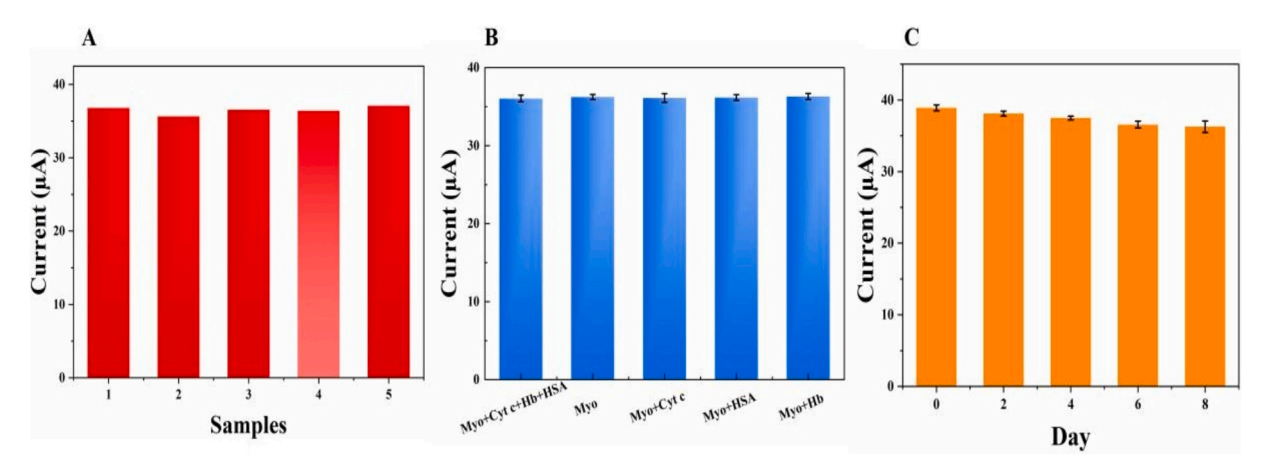


Fig. 5. (A) DPV measurements of five different GCEs through the same build process (10 ng/mL Myo). (B) Interference detections:10 ng/mL Myo, Myo + Cyt c, Myo + HSA, Myo + HB. (C) Immunosensor stability tests (10 ng/mL Myo); (Error bar = SD, n = 3).

immunosensor was successfully prepared for the detection of Myo, a promising biomarker for the early diagnosis of AMI. The sensing platform was constructed by incubating the Myo antibody on GCE modified with Au/Co-BDC@MD, which provided a large surface area for antibody immobilization and enhanced electron transfer, and the optimization of the experimental parameters, such as pH (7.4), the concentration of Au/ Co-BDC@MD (3.5 mg/mL) and the incubation time (50 min), significantly improved the performance of the immunosensor. Running under optimized parameters, the developed sensing platform showed a linear detection of Myo in the range of 10 fg/mL \sim 10 ng/mL and an LOD of 10.03 fg/mL. The immunosensor also showed high selectivity, with an RSD of 0.23 % in the presence of interfering substances. In addition, the immunosensor showed good reproducibility (RSD = 1.31 %) and stability, maintaining 93.24 % of the initial response after 8 days of storage at 4 °C.The proposed immunosensor has the advantage of better analytical performance and lower detection limit compared to other reported Myo assays. The prepared immunosensor achieves sensitive and stable detection of Myo, which has potential application for monitoring other biomarkers for early and accurate diagnosis of various diseases. Future research should focus on integration into portable devices for real-time Myo monitoring and early diagnosis of AMI.

CRediT authorship contribution statement

Qiaozhi Yang: Writing – review & editing, Writing – original draft, Validation, Methodology, Investigation, Conceptualization. Weiyun Chen: Writing – review & editing, Supervision, Investigation. Jiaxin Shi: Writing – review & editing. Xin Huang: Project administration, Funding acquisition. Luwei Zhang: Funding acquisition. Yunhan Zhang: Writing – review & editing. Yixuan Wang: Writing – review & editing. Yudong Wu: Project administration, Funding acquisition. Xin Li: Project administration, Methodology, Funding acquisition, Conceptualization. Kebin Xu: Project administration, Methodology, Funding acquisition, Conceptualization, Conceptualization, Conceptualization, Funding acquisition, Conceptualization, Methodology, Funding acquisition, Conceptualization.

Declaration of competing interest

The authors declare that they have no known competing financial interests or personal relationships that could have appeared to influence the work reported in this paper.

Acknowledgments

This work was supported by the National Natural science foundaion of china under Grant 62433007, Basic Research Projects of Liaoning Provincial Department of Education (No. LJ222410164024, LJ212510164032 and No. LJ222410164030), Shenyang Young and Middle aged Science and Technology Talents Cultivation Special Project for Returning Overseas Youth (No. RC230088). Doctoral Research Startup Projects of the Natural Science Foundation of Liaoning Province (No. 2024-BS-280). Liaoning Provincial Department of Science and Technology Program Project (No. 2024JH2/102600237) Graduate Science and Technology Innovation Fund Project of Shenyang Medical University (No. Y20240532 and No.Y20240535).

Appendix A. Supplementary data

Supplementary data to this article can be found online at https://doi.org/10.1016/j.microc.2025.114831.

Data availability

Data will be made available on request.

References

- X. Mi, H. Li, Y. Tu, An aptamer biosensing strategy for label-free assay of dual acute myocardial infarction biomarkers built upon AuNPs/Ti3C2-MXenes, CHEMOSENSORS 11 (2023), https://doi.org/10.3390/chemosensors11030157.
- [2] E.V. Suprun, A.L. Shilovskaya, A.V. Lisitsa, T.V. Bulko, V.V. Shumyantseva, A. I. Archakov, Electrochemical Immunosensor based on metal nanoparticles for cardiac myoglobin detection in human blood plasma, ELECTROANALYSIS 23 (2011) 1051–1057. https://doi.org/10.1002/elan.201000668.
- [3] J. Chen, F. Ran, Q. Chen, D. Luo, W. Ma, T. Han, C. Wang, C. Wang, A fluorescent biosensor for cardiac biomarker myoglobin detection based on carbon dots and deoxyribonuclease I-aided target recycling signal amplification, RSC Adv. 9 (2019) 4463–4468, https://doi.org/10.1039/c8ra09459d.
- [4] J.A. Ribeiro, C.M. Pereira, A.F. Silva, M.G.F. Sales, Electrochemical detection of cardiac biomarker myoglobin using polyphenol as imprinted polymer receptor, Anal. Chim. Acta 981 (2017) 41–52, https://doi.org/10.1016/j.aca.2017.05.017.
- [5] S.M. Taghdisi, N.M. Danesh, M. Ramezani, A.S. Emrani, K. Abnous, A novel electrochemical aptasensor based on Y-shape structure of dual-aptamercomplementary strand conjugate for ultrasensitive detection of myoglobin, Biosens. Bioelectron. 80 (2016) 532–537, https://doi.org/10.1016/j. bios.2016.02.029.
- [6] M.R.K. Pur, M. Hosseini, F. Faridbod, M.R. Ganjali, Highly sensitive label-free electrochemiluminescence aptasensor for early detection of myoglobin, a biomarker for myocardial infarction, Microchim. Acta 184 (2017) 3529–3537, https://doi.org/10.1007/s00604-017-2385-y.
- [7] O.V. Gnedenko, Y.V. Mezentsev, A.A. Molnar, A.V. Lisitsa, A.S. Ivanov, A. I. Archakov, Highly sensitive detection of human cardiac myoglobin using a reverse sandwich immunoassay with a gold nanoparticle-enhanced surface plasmon resonance biosensor, Anal. Chim. Acta 759 (2013) 105–109, https://doi.org/10.1016/j.aca.2012.10.053.
- [8] V. Kumari, P. Gulati, P. Mishra, S.S. Islam, Porous Silicon Myoglobin Immunosensor, Adv. Sci. Lett. 20 (2014) 1574–1577, https://doi.org/10.1166/ asl/2014/5596
- [9] M. Li, Y. Wu, C. Ke, Z. Song, M. Zheng, Q. Yu, H. Zhu, H. Guo, H. Sun, M. Liu, An ultrasensitive unlabeled electrochemical immunosensor for the detection of cardiac troponin I based on Pt/Au-B,S,N-rGO as the signal amplification platform, Talanta 270 (2024), https://doi.org/10.1016/j.talanta.2023.125546.
- [10] F. Xu, Q.-Y. Ai, A.-J. Wang, L.-P. Mei, P. Song, W. Liu, J.-J. Feng, T.Y. Cheang, Pronounced signal enhancement with gourd-shaped hollow PtCoNi bunched nanochains for electrochemical immunosensing of alpha-fetoprotein, Sensors Actuators B-Chem. 422 (2025), https://doi.org/10.1016/j.snb.2024.136608.
- [11] C.-L. Lv, C. Tang, H. Zhou, A.-J. Wang, J.-J. Feng, T.Y. Cheang, Self-supported PtPdMnCoFe high-entropy alloy with nanochain-like internetworks for ultrasensitive electrochemical immunoassay of biomarker, Sensors Actuators B-Chem. 401 (2024), https://doi.org/10.1016/j.snb.2023.135041.
- [12] Y.-Y. Shi, Y.-L. Zhong, A.-J. Wang, L.-P. Mei, P. Song, T. Zhao, J.-J. Feng, Trimetallic PtPdCo nanoalloy on hollow porous N-doped carbon fibers: a highperformance electrochemical immunosensor for procalcitonin detection in SIRS diagnosis, Microchim. Acta 192 (2025), https://doi.org/10.1007/s00604-025-07089-x
- [13] S.M. Khoshfetrat, P. Hashemi, A. Afkhami, A. Hajian, H. Bagheri, Cascade electrochemiluminescence-based integrated graphitic carbon nitride-encapsulated metal-organic framework nanozyme for prostate-specific antigen biosensing, Sensors Actuators B-Chem. 348 (2021), https://doi.org/10.1016/j. spb. 2021.130658
- [14] S.M. Khoshfetrat, P.S. Dorraji, L. Fotouhi, M. Hosseini, F. Khatami, H.R. Moazami, K. Omidfar, Enhanced electrochemilluminescence biosensing of gene-specific methylation in thyroid cancer patients' plasma based integrated graphitic carbon nitride-encapsulated metal-organic framework nanozyme optimized by central composite design, Sensors Actuators B-Chem. 364 (2022), https://doi.org/10.1016/j.snb.2022.131895.
- [15] S. Roy, K.A. Deo, K.A. Singh, H.P. Lee, A. Jaiswal, A.K. Gaharwar, Nano-bio interactions of 2D molybdenum disulfide, Adv. Drug Deliv. Rev. 187 (2022), https://doi.org/10.1016/j.addr.2022.114361.
- [16] J. Lu, M. Chen, L. Dong, L. Cai, M. Zhao, Q. Wang, J. Li, Molybdenum disulfide nanosheets: from exfoliation preparation to biosensing and cancer therapy applications, Colloids & Surf B-Biointerfaces 194 (2020), https://doi.org/10.1016/ i.colsurfb.2020.111162.
- [17] L. Gong, L. Feng, Y. Zheng, Y. Luo, D. Zhu, J. Chao, S. Su, L. Wang, Molybdenum disulfide-based Nanoprobes: preparation and sensing application, BIOSENSORS-BASEL 12 (2022), https://doi.org/10.3390/bios12020087.
- [18] Y. Jiao, Z. Huang, M. Chen, X. Zhou, H. Lu, B. Wang, X. Dai, A label-free amperometric immunosensor with improved electrocatalytic 3D braided AuPtCu-SWCNTs@MoS2-rGO for human growth differentiation factor-15 detection, Anal. Methods 14 (2022) 1420–1429, https://doi.org/10.1039/d1ay02198b.
- [19] X. Lin, Y. Ni, S. Kokot, Electrochemical cholesterol sensor based on cholesterol oxidase and MoS2-AuNPs modified glassy carbon electrode, Sensors Actuators B Chem. 233 (2016) 100–106.
- [20] S. Ahmad, I. Khan, A. Husain, A. Khan, A.M. Asiri, Electrical conductivity based Ammonia sensing properties of Polypyrrole/MoS2 nanocomposite, POLYMERS 12 (2020), https://doi.org/10.3390/polym12123047.
- [21] C. Meng, X. Chen, Y. Gao, Q. Zhao, D. Kong, M. Lin, X. Chen, Y. Li, Y. Zhou, Recent modification strategies of MoS2 for enhanced Electrocatalytic hydrogen evolution, MOLECULES 25 (2020), https://doi.org/10.3390/molecules25051136.

- [22] J. Das, K. Jo, J.W. Lee, H. Yang, Electrochemical immunosensor using paminophenol redox cycling by hydrazine combined with a low background current, Anal. Chem. 79 (2007) 2790–2796, https://doi.org/10.1021/ac0622911.
- [23] Q. Zha, F. Yuan, G. Qin, Y. Ni, Cobalt-based MOF-on-MOF two-dimensional heterojunction nanostructures for enhanced oxygen evolution reaction Electrocatalytic activity, Inorg. Chem. 59 (2020) 1295–1305, https://doi.org/ 10.1021/acs.inorgchem.9b03011.
- [24] D. Zhu, J. Liu, Y. Zhao, Y. Zheng, S.-Z. Qiao, Engineering 2D metal-organic framework/MoS2 Interface for enhanced alkaline hydrogen evolution, SMALL 15 (2019), https://doi.org/10.1002/smll.201805511.
- [25] S.M. Khoshfetrat, P.S. Dorraji, M. Shayan, F. Khatami, K. Omidfar, Smartphone-based electrochemiluminescence for visual simultaneous detection of RASSF1A and SLC5A8 tumor suppressor gene methylation in thyroid cancer patient plasma, Anal. Chem. 94 (2022) 8005–8013, https://doi.org/10.1021/acs.analchem.2c01132
- [26] S.M. Khoshfetrat, P. Hashemi, A. Afkhami, A. Hajian, H. Bagheri, Cascade electrochemiluminescence-based integrated graphitic carbon nitride-encapsulated metal-organic framework nanozyme for prostate-specific antigen biosensing, Sensors Actuators B-Chem. 348 (2021), https://doi.org/10.1016/j. spb.2021.130658.
- [27] S.M. Khoshfetrat, H. Khoshsafar, A. Afkhami, M.A. Mehrgardi, H. Bagheri, Enhanced visual wireless Electrochemiluminescence Immunosensing of prostatespecific antigen based on the Luminol loaded into MIL-53(Fe)-NH2 accelerator and hydrogen evolution reaction mediation, Anal. Chem. 91 (2019) 6383–6390, https://doi.org/10.1021/acs.analchem.9b01506.
- [28] V. Mani, B.V. Chikkaveeraiah, V. Patel, J.S. Gutkind, J.F. Rusling, Ultrasensitive Immunosensor for Cancer biomarker proteins using gold nanoparticle film electrodes and multienzyme-particle amplification, ACS Nano 3 (2009) 585–594, https://doi.org/10.1021/nn800863w.
- [29] X. Liu, C. Fang, J. Yan, H. Li, Y. Tu, A sensitive electrochemiluminescent biosensor based on AuNP-functionalized ITO for a label-free immunoassay of C-peptide, BIOELECTROCHEMISTRY 123 (2018) 211–218, https://doi.org/10.1016/j. bioelechem.2018.05.010.
- [30] X. Liu, H. Huang, G. Liu, W. Zhou, Y. Chen, Q. Jin, J. Ji, Multidentate zwitterionic chitosan oligosaccharide modified gold nanoparticles: stability, biocompatibility and cell interactions, NANOSCALE 5 (2013) 3982–3991, https://doi.org/10.1039/ c3nr00284e
- [31] P. Jiang, Y. Wang, L. Zhao, C. Ji, D. Chen, L. Nie, Applications of gold nanoparticles in non-optical Biosensors, NANOMATERIALS 8 (2018), https://doi.org/10.3390/ nano8120977.
- [32] S. Su, H. Sun, W. Cao, J. Chao, H. Peng, X. Zuo, L. Yuwen, C. Fan, L. Wang, Dual-target electrochemical biosensing based on DNA structural switching on gold nanoparticle-decorated MoS2 Nanosheets, ACS Appl. Mater. Interfaces 8 (2016) 6826–6833. https://doi.org/10.1021/acsami.5b12833.
- [33] Y. Liu, B. Sun, Y. Wu, H. Li, D. Li, Q. Dang, S. Liu, X. Da, M. Zhou, Y. Lv, X. Wang, L. Yang, A novel electrochemical immunosensor based on AuNPs/PNR/CS@ MWCNTs-COOH for rapid detecting warning markers-BNP of heart failure caused by myocardial infarction, Microchem. J. 207 (2024) 111654, https://doi.org/10.1016/j.cep.2024.11654.
- [34] L. Bao, Z. Wang, J. Kang, H. He, B. Sun, Y. Liu, M. Zhou, Q. Dang, D. Li, Y. Wu, H. Li, L. Yang, H. Wang, An electrochemical immunosensor based on MXene for highly sensitive rapid detection of acute heart failure biomarker-BNP, Microchem. J. 213 (2025) 113564. https://doi.org/10.1016/j.microc.2025.113564.
- J. 213 (2025) 113564, https://doi.org/10.1016/j.microc.2025.113564.
 [35] B. Sun, L. Bao, Y. Sun, J. Liu, Y. Wu, H. Li, S. Yu, Y. Liu, Q. Dang, L. Yang, Electrochemical immunosensor based on ferrocene derivatives amplified signal for detection of acute myocardial infarction warning biomarker-cTnI, Microchem. J. 199 (2024) 110057, https://doi.org/10.1016/j.microc.2024.110057.
- [36] Y. Liu, B. Sun, Y. Wu, H. Wang, H. Li, Q. Dang, W. Wang, M. Zhou, X. Da, H. He, J. Kang, L. Yang, X. Pu, Q. Ma, Fabricating electrochemical immunosensor based on magnetic multi-walled carbon nanotubes for rapid detection of early warning marker of acute myocardial infarction-Mb, Microchem. J. 215 (2025) 114449, https://doi.org/10.1016/j.microc.2025.114449.
- [37] Z. Chang, Q. Zhao, Label-free electrochemical immunosensor determination of CA125 using Cu2+ and hemin dual-functionalized PEI/SiO2 nanoparticles, Microchem. J. (2025) 114543, https://doi.org/10.1016/j.microc.2025.114543.
- [38] X. Sun, Z. Wang, S. Wang, S. Wang, H. Jiang, J. Zhang, T. Liu, Q. Liu, P. Wang, D. Zhang, K. Feng, Y. Li, F. Tang, Ultrasensitive electrochemical immunosensor integrated trimetallic PtCuRu alloy and N-rich interpenetrating twin porous carbon for quantitative detection of cTnI, Microchem. J. 213 (2025) 113594, https://doi.org/10.1016/j.microc.2025.113594.
- [39] F. Pei, P. Wang, E. Ma, Q. Yang, H. Yu, C. Gao, Y. Li, Q. Liu, Y. Dong, A sandwich-type electrochemical immunosensor based on RhPt NDs/NH2-GS and au NPs/PPy NS for quantitative detection hepatitis B surface antigen, BIOELECTROCHEMISTRY 126 (2019) 92–98, https://doi.org/10.1016/j.bioelechem.2018.11.008.
- [40] H. Zhao, X. Du, H. Dong, D. Jin, F. Tang, Q. Liu, P. Wang, L. Chen, P. Zhao, Y. Li, Electrochemical immunosensor based on au/co-BDC/MoS2 and DPCN/MoS2 for the detection of cardiac troponin I, Biosens. Bioelectron. 175 (2021), https://doi. org/10.1016/j.bios.2020.112883.
- [41] Z. Zhang, J. Liu, Y. Li, J. Dong, J. Qiu, C. Li, A novel electrochemical immunosensor based on rifter-like Ni-TCPP(Fe) nanosheets and PSS-functionalized graphene for ultrasensitive detection of H-FABP, J. Solid State Electrochem. 28 (2024) 389–398, https://doi.org/10.1007/s10008-023-05482-1.
- [42] Y. Liu, G. He, H. Liu, H. Yin, F. Gao, J. Chen, S. Zhang, B. Yang, Electrochemical immunosensor based on AuBP@Pt nanostructure and AuPd-PDA nanozyme for

- ultrasensitive detection of APOE4, RSC Adv. 10 (2020) 7912–7917, https://doi. org/10.1039/d0ra00298d.
- [43] A. Ahmadi, S.M. Khoshfetrat, S. Kabiri, L. Fotouhi, P.S. Dorraji, K. Omidfar, Impedimetric paper-based enzymatic biosensor using electrospun cellulose acetate nanofiber and reduced graphene oxide for detection of glucose from whole blood, IEEE Sensors J. 21 (2021) 9210–9217, https://doi.org/10.1109/ ISEN 2021 3053033
- [44] M.F. Mousavi, M. Amiri, A. Noori, S.M. Khoshfetrat, A prostate specific antigen Immunosensor based on biotinylated-antibody/Cyclodextrin inclusion complex: fabrication and electrochemical studies, Electroanalysis 29 (2017) 2818–2831, https://doi.org/10.1002/elan.201700363.
- [45] M. Acerce, D. Voiry, M. Chhowalla, Metallic 1T phase MoS2 nanosheets as supercapacitor electrode materials, Nat. Nanotechnol. 10 (2015) 313–318, https://doi.org/10.1038/NNANO.2015.40.
- [46] F. Momeni, S.M. Khoshfetrat, K. Zarei, Electrochemical Sandwich-type Aptasensor based on the multifunctional catechol-loaded au/MIL-53(Fe) for detection of cardiac troponin I, ACS Appl. Nano Mater. 6 (2023) 19239–19248, https://doi. org/10.1021/acsanm.3c03705.
- [47] F. Momeni, S.M. Khoshfetrat, H. Bagheri, K. Zarei, Ti3C2 MXene-based nanozyme as coreaction accelerator for enhancing electrochemiluminescence of glucose biosensing, Biosens. Bioelectron. 250 (2024), https://doi.org/10.1016/j. bios. 2024.116078.
- [48] V. Mani, B.V. Chikkaveeraiah, V. Patel, J.S. Gutkind, J.F. Rusling, Ultrasensitive Immunosensor for Cancer biomarker proteins using gold nanoparticle film electrodes and multienzyme-particle amplification, ACS Nano 3 (2009) 585–594, https://doi.org/10.1021/nn800863w.
- [49] S.M. Khoshfetrat, M. Yari, P.S. Dorraji, F. Jalali, Synergistic effects of nanoporous structure of glassy carbon electrode and electropolymerization of catechol film on the electrocatalytic oxidation of hydrazine, J. Electrochem. Soc. 170 (2023) 077511, https://doi.org/10.1149/1945-7111/ace7f9.
- [50] S.M. Khoshfetrat, M.A. Mehrgardi, Electrochemical genotyping of single-nucleotide polymorphisms by using monobase-conjugated modified nanoparticles, ChemElectroChem 1 (2014) 779–786, https://doi.org/10.1002/celc.201300221.
- [51] E. Suprun, T. Bulko, A. Lisitsa, O. Gnedenko, A. Ivanov, V. Shumyantseva, A. Archakov, Electrochemical nanobiosensor for express diagnosis of acute myocardial infarction in undiluted plasma, Biosens. Bioelectron. 25 (2010) 1694–1698, https://doi.org/10.1016/j.bios.2009.12.009.
- [52] G. Rabbani, E. Ahmad, M.E. Khan, A.U. Khan, M.A. Zamzami, A. Ahmad, S.K. Ali, A.H. Bashiri, W. Zakri, Synthesis of carbon nanotubes-chitosan nanocomposite and immunosensor fabrication for myoglobin detection: an acute myocardial infarction biomarker, Int. J. Biol. Macromol. 265 (2024), https://doi.org/10.1016/j.iibiomac.2024.130616.
- [53] L. Sun, W. Li, M. Wang, W. Ding, Y. Ji, Development of an electrochemical impedance Immunosensor for myoglobin determination, Int. J. Electrochem. Sci. 12 (2017) 6170–6179, https://doi.org/10.20964/2017.07.72.
- [54] S. Singh, S.K. Tuteja, D. Sillu, A. Deep, C.R. Suri, Gold nanoparticles-reduced graphene oxide based electrochemical immunosensor for the cardiac biomarker myoglobin, Microchim. Acta 183 (2016) 1729–1738, https://doi.org/10.1007/ s006.04-016-1803-x.
- [55] R. Khan, M. Pal, A.V. Kuzikov, T. Bulko, E.V. Suprun, V.V. Shumyantseva, Impedimetric immunosensor for detection of cardiovascular disorder risk biomarker, Mater. Sci. Eng. C 68 (2016) 52–58, https://doi.org/10.1016/j. msec 2016.05.107
- [56] S.K. Tuteja, R. Chen, M. Kukkar, C.K. Song, R. Mutreja, S. Singh, A.K. Paul, H. Lee, K.-H. Kim, A. Deep, C.R. Suri, A label-free electrochemical immunosensor for the detection of cardiac marker using graphene quantum dots (GQDs), Biosens. Bioelectron. 86 (2016) 548–556, https://doi.org/10.1016/j.bios.2016.07.052.
- [57] B. Wang, S.M. Khoshfetrat, H. Mohamadimanesh, Peroxidase-like manganese oxide nanoflowers-delaminated Ti3C2 MXene for ultrasensitive dual-mode and real-time detection of H2O2 released from cancer cells, Microchem. J. 207 (2024), https://doi.org/10.1016/j.microc.2024.111796.
- [58] S.M. Khoshfetrat, M. Nabavi, S. Mamivand, Z. Wang, Z. Wang, M. Hosseini, Ionic liquid-delaminated Ti3C2 MXene nanosheets for enhanced electrocatalytic oxidation of tryptophane in normal and breast cancer serum, Microchim. Acta 192 (2025), https://doi.org/10.1007/s00604-025-06968-7.
- [59] S.M. Khoshfetrat, M. Moradi, H. Zhaleh, M. Hosseini, Multifunctional methyl orange-delaminated Ti3C2 MXene for non-enzymatic/metal-free electrochemical detection of hydrogen peroxide and hydrazine, Microchem. J. 205 (2024) 111382, https://doi.org/10.1016/j.microc.2024.111382.
 [60] S.M. Khoshfetrat, M. Motahari, S. Mirsian, 3D porous structure of ionic liquid-
- [60] S.M. Khoshfetrat, M. Motahari, S. Mirsian, 3D porous structure of ionic liquid-delaminated Ti3C2 MXene nanosheets for enhanced electrochemical sensing of tryptophan in real samples, Sci. Rep. 15 (2025), https://doi.org/10.1038/s41598-025-91773-8.
- [61] S.M. Khoshfetrat, In situ synthesis of nickel-substituted zeolitic metal-organic framework on Ti3C2 MXene for enhanced electrocatalytic sensing of L-tryptophan, J. Electroanal. Chem. 992 (2025), https://doi.org/10.1016/j. ielechem.2025.119215.
- [62] S.M. Khoshfetrat, K. Fasihi, F. Moradnia, H.K. Zaidan, E. Sanchooli, A label-free multicolor colorimetric and fluorescence dual mode biosensing of HIV-1 DNA based on the bifunctional NiFe2O4@UiO-66 nanozyme, Anal. Chim. Acta 1252 (2023), https://doi.org/10.1016/j.aca.2023.341073.
- [63] S.M. Khoshfetrat, S. Mamivand, G.B. Darband, Hollow-like three-dimensional structure of methyl orange-delaminated Ti3C2 MXene nanocomposite for highperformance electrochemical sensing of tryptophan, Microchim. Acta 191 (2024), https://doi.org/10.1007/s00604-024-06622-8.